Mine Water and the Environment (2020) 39:256–267
https://doi.org/10.1007/s10230-020-00675-w

TECHNICAL ARTICLE

Experimental Investigation of the Pressure and Water Pressure Responses of an Inclined Shaft Wall During Grouting

Gailing Zhang[1] · Shichong Yuan[1,2] · Wanghua Sui[1] · Ziwei Qian[1]

Received: 1 April 2019 / Accepted: 2 March 2020 / Published online: 10 March 2020

Abstract

A scale model test with a geometric scale of 1:20 was carried out to simulate chemical grouting in a geological prototype of the auxiliary inclined shaft of the Jinjitan coal mine, Shaanxi Province, to address water and sand inrush accidents. The pressure responses in the surrounding sand layers to grouting of an inclined shaft was experimentally investigated using soil pressure and pore water pressure sensors. Grout propagation was observed by slicing the stabilized mass after grouting. The results show that grouting of the roof, side wall, and floor of the inclined shaft caused pressures to both increase and decrease; after the slurry fully gelled, the pressure on the roof and side wall of the inclined shaft was effectively released, but accumulated on the floor. The water pressure on the roof and side wall of the inclined shaft went through three stages: low amplitude fluctuations, high amplitude fluctuations, and a sudden drop. The floor water pressure experienced stages of pressure fluctuation, maintenance, and recovery. The propagation and solidification of the slurry increased the pressure on the shaft wall. By analyzing the solidified grouted mass, we found that contact among particles within the penetration radius can be classified into three types: a gelled slurry skeleton, an integrated granular particle and slurry skeleton, and a granular particle skeleton. Moreover, the reinforcement mechanism of grouting is mainly fracturing and permeation. The results imply that the designed grouting pressure in the floor should be slightly less than in the roof and side wall to avoid secondary failure of the floor. During actual grouting, fracturing occurs first under high grouting pressure, while permeation occurs as grouting pressure decreases.

Keywords Water and sand inrush · Scale model test · Underground mine

Introduction

Water and sand inrush events due to mine shaft wall rupture has caused safety issues and substantial economic losses, especially in the coal mines of China. After a rupture has taken place, grouting behind the wall is a common and effective practice. Grout propagation must be well understood to evaluate the effectiveness of grouting and to improve the process. Methods to investigate grouting mechanisms include theoretical analyses, numerical simulations, scale model tests, and in situ measurements. Theoretical analysis often assumes simplified conditions, such as Maag's formula for homogenous and isotropic soil and Newtonian fluids (Maag 1938), radial flow equations for parallel fractures, and Newtonian or Binghamian fluids (Amadei and Savage 2001; Dai and Bird 1981; Gustafson et al. 2013; Xiao et al. 2017). However, these assumptions and approximations can be inaccurate when used to describe grouting mechanisms (Håkansson 1993; Ruan 2005). Since this grout propagation

Gailing Zhang and Shichong Yuan contributed equally to this work.

Electronic Supplementary Material The online version of this article (https://doi.org/10.1007/s10230-020-00675-w) contains supplementary material, which is available to authorized users.

✉ Wanghua Sui
suiwanghua@cumt.edu.cn

Gailing Zhang
gailing-zhang@cumt.edu.cn

Shichong Yuan
yuanshichong@cumt.edu.cn

Ziwei Qian
ziweidav@163.com

[1] School of Resources and Geosciences, China University of Mining and Technology, 1 University Rd, Xuzhou 221116, Jiangsu, China

[2] North China Engineering Investigation Institute Co. Ltd., Shijiazhuang 050021, Hebei, China

is difficult to observe in-situ (since it is behind a concealed wall), it is generally studied using scale model tests and numerical simulations. Since numerical simulations are based on many physical approximations, this approach also cannot sufficiently simulate the grouting conditions. Therefore, by elimination, scale modeling is the best alternative for investigating grouting and reinforcement mechanisms that cannot be easily observed in situ (Cheng et al. 2018; Mohammed et al. 2015). Scale models are now extensively used to obtain insights into the propagation and reinforcement mechanism of grouting in soil and rock masses, aided by the recent development of digital photography and image processing (Funehag and Thörn 2018; Minto et al. 2016). The permanence, major effects, and mathematical models of injected chemical grout in soil and rock masses with flowing water have been studied by Karol (2003), Krizek and Perez (1985), Liang et al. (2019), Sui et al. (2015), Wang (2011) and Xu et al. (2019b).

High potential energy (e.g. a high water table) can cause hazardous water and sand inrushes when a pathway exists due to faults or fractures in the rock mass (Castro et al. 2017; Vallejos et al. 2017), which makes grouting even more difficult. The grouting mechanism in sand aquifers around deep vertical shafts has been widely studied in eastern China, where almost all shafts are vertically constructed (Cui 1998; Ni et al. 2005; Xu et al. 2019a). However, there have been few studies regarding the grouting mechanism for inclined shaft wall ruptures. Most coal mines in western China have shallow burials; therefore, inclined shafts are constructed for transporting vehicles and supporters. The vertical shafts in eastern China are mainly surrounded by fluvial and lacustrine sand and clay layers, while the inclined shafts in western China are generally covered by aeolian sand. The soil layers have different compositions and physico-mechanical properties, resulting in different problems for water and sand inrush disaster treatment. Related studies have shown that the inclination of structures and fractures significantly influences the effectiveness of grouting for mitigating water and sand inrush (Cochard and Ancey 2009; Haza et al. 2013; Luo et al. 2009; Qian et al. 2018; Yu et al. 2014).

Grouting has also been successfully used to remediate water and sand inrush resulting from the rupturing of shallow buried shafts in the west (Qian et al. 2018; Yuan et al. 2018, 2019). As the grout blocks the water inflow pathway, the grouts propagate in the sand layers behind the wall and disturb the ruptured shaft wall. The state of stress and pore water pressure at different positions in the shaft wall will be changed during the propagation and solidification of grout. Guo (2010) proposed three diffusion modes when the grout is injected into a closed chamber with high pressure. During the process of sand compaction, infiltration, and fracturing, variations in the diffusion concentration of chemical grouts in sand greatly influences its permeability (Zhang 2011). These changes in the pressure and water pressure can cause further deformation and even failure of the shaft wall. For example, during grouting of the Jinjitan coal mine's inclined shaft, the grouting caused a floor heave of more than 100 mm. One or 2 mm fractures in the side wall and roof increased to 20 mm or even larger. A grouting pressure design that does not cause secondary failure of the shaft wall and ensures the adequate propagation of grouts is particularly important. Therefore, changes in the pressure and water pressure acting on the shaft wall and in the surrounding soil layers due to grouting are important for understanding the mechanism of grouting and for determining the grouting scheme.

A scale model for grouting behind an inclined shaft wall was designed based on grouting behind the auxiliary inclined shaft wall of the Jinjitan coal mine. The purpose of this study was to provide insight into the mechanism of grouting behind an inclined shaft wall and provide a reference for grouting design for inclined shaft ruptures.

Engineering Geological Conditions and Problems

Geological Conditions

The Jinjitan coal mine is located in Yulin City, Shaanxi Province, on the southeastern edge of the Mu Us Desert (Supplemental Fig. 1). The stratigraphy consists of the Triassic Yongping Formation (T_3y), the Jurassic Xiafuxian (J_1f), Yan'an (J_2y), Zhiluo (J_2z), Anding (J_2a) Formations, the Neogene Baode Formation (N_2b), the Quaternary Lishi Formation (Q_2l), the Pleistocene Sarawusu Formation (Q_3s), and Holocene aeolian deposits (Q_4^{eol}). The Holocene sand layer (between 0 and 46.60 m thick, averaging 8.02 m) is deposited over other strata as fixed and a few semifixed dunes; these dunes have an unconformity contact with the underlying strata. The lithology is mainly well-graded fine sand and silt with a uniform texture and a yellow color, and contains plant roots and black minerals with a loose structure. The geological structure of the mine is monoclinic, with an inclination angle of less than 1° toward the northwest. The productive coal seam is in the Jurassic System without magma activity or folds. The mine has a production capacity of 12.0 Mt/a, a field area of 107.89 km^2, an average coal seam thickness of 8.0 m, and a buried depth of 130–430 m.

The auxiliary inclined shaft of the Jinjitan Mine has a slope of 5°, with an inclined length of 3028 m, and a depth at the bottom of 263.9 m. The unconsolidated Quaternary Salawusu (Q_3s) and Lishi (Q_2l) Formations are crossed by the inclined shaft, which consists of fine sand, medium sand, and loess from top to bottom; the loess layers are entrained

in a 1.83 m thick saturated sand layer. Figure 1 shows the types of soil layers and their relative locations against the auxiliary inclined shaft. The upper fine and medium sand aquifers are the Quaternary unconfined aquifer, with a water level depth of 3.27 m, which is recharged by atmospheric precipitation. There is a thin confined aquifer beneath the loess. The specific capacity of water yield is between 0.084 and 0.92 L/(s•m), which represents weak-to-medium water abundance.

Water and Sand Inrush Accidents and Treatments

On July 28, 2016, it was found that the sand content continued to increase in the sump flow at the 230–320 m ditches of the auxiliary inclined shaft. The floor had cracked, the roof was cracked and drenched, and the maximum flow rate reached 72 m^3/h. The sand content reached 16%. The deformation of the shaft wall at 260 m reached 422.5 mm, indicating that the shaft wall could collapse at any time. On August 17, 2016, there were 11 collapse pits on the surface, 240–290 m above the inclined shaft (Fig. 2).

The analysis revealed that the water and sand flowed directly into the auxiliary inclined shaft from the sand aquifers around the auxiliary inclined shaft, through cracks in the floor. Therefore, the aquifers behind the side wall were the source, and the side wall was the main pathway for the water and sand. Grouting was extensively performed by drilling boreholes in the auxiliary inclined shaft side. As the effective propagation range of the slurry increased, the side and the floor corner formed a consolidated mass, which blocked

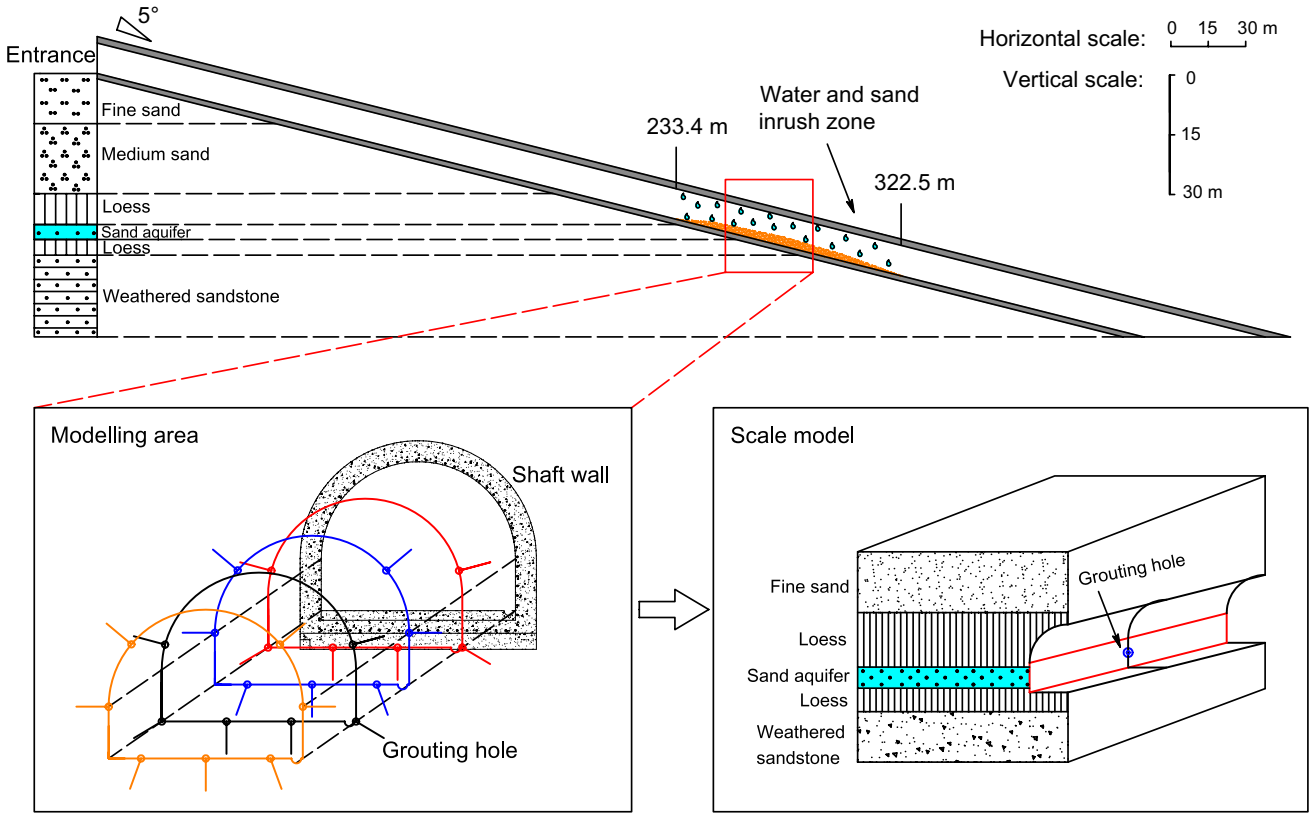

Fig. 1 Schematic of surrounding soil and rock masses and grouting engineering of the inclined shaft

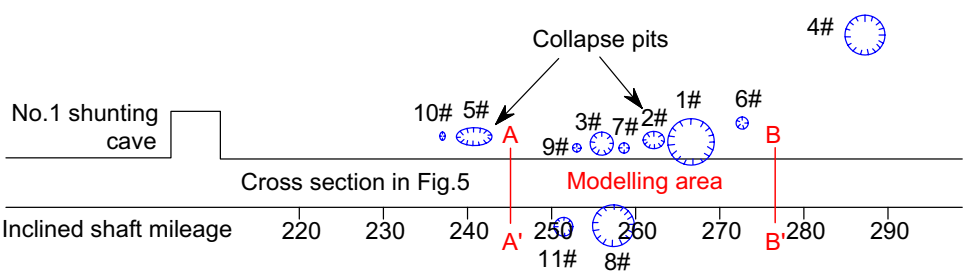

Fig. 2 Subsidence pits due to water and sand inrush of the inclined shaft

the source and pathway of the water and sand. The grouting simultaneously blocked the pathway and sealed the source. Figure 3 shows the measured changes in the water inflow, sand content, and shaft wall deformation during treatment. Supplemental Figure 2 shows that the grouting caused severe floor heave deformation of the inclined shaft. The details of the treatment can be found in Qian et al. (2018) and Yuan et al. (2018, 2019).

After grouting blocked the water and sand, the water pressure behind the wall rose, and new points of water inflow appeared in weak points of the wall. Therefore, it was decided that the pressure on the wall during grouting and the water pressure in the surrounding sand layers as well as the propagation of the slurry behind the wall must be further studied.

Materials and Methods

Aeolian Sand

The aeolian sand used in the test was obtained from the Jinjitan coal mine in the Yuyang District, Yulin City, Shaanxi Province. Supplemental Figure 3 shows that the aeolian sand was mainly composed of quartz and feldspar with a small content of heavy minerals, such as hornblende, epidote, and garnet, and clay minerals, mostly illite. Supplemental Figure 4 shows the particle size distribution of the aeolian sand, indicating that the particle size is homogenous and poorly graded; Table 1 lists its geotechnical properties.

Water

In the experiment, water with similar pH values was used. Groundwater in the sand aquifer behind the shaft wall from the Jinjitan coal mine has a pH of 7.85 and a total dissolved solids (TDS) value of 507.2–506.7 mg/L. The concentrations of SO_4^{2-}, Cl^-, and Mg^{2+} ions are 150.3, 46.8, and 11.7 mg/L, respectively. The water used in the experiment had a pH of 7.56–7.80 and a TDS value of 397–584 mg/L, according to the Xuzhou water supply center, which indicated that it could be used to replace groundwater with similar properties.

Grouts

The chemical grout used for grouting the auxiliary inclined shaft was a modified urea–formaldehyde resin (Liquid A) mixed with a 5% oxalic acid solution (Liquid B). The mixing ratio of the modified urea–formaldehyde resin and oxalic acid and the ambient temperature are important factors that affect the gel time. The ratios of the modified urea–formaldehyde resin to the oxalic acid solution are 1:1, 2:1, 3:1, 4:1, and 5:1 by volume. Supplemental Figure 5 shows the

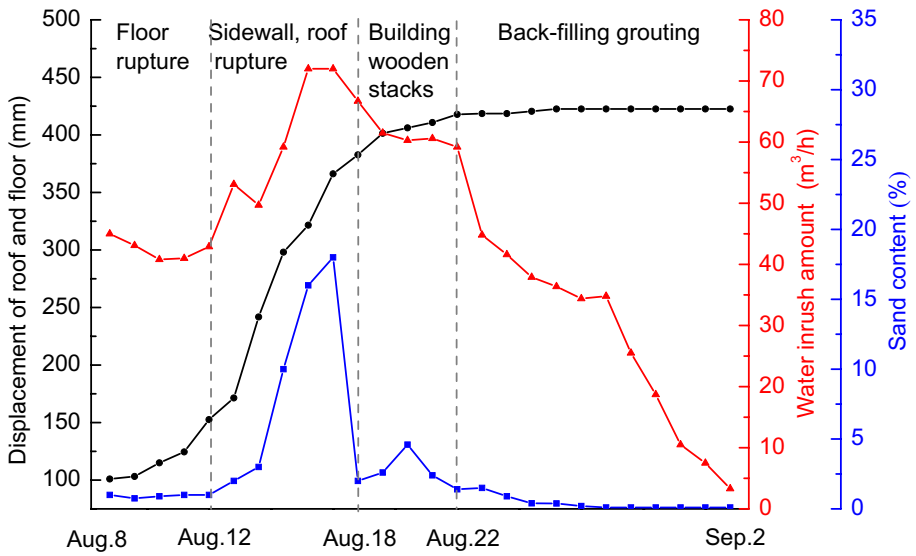

Fig. 3 Water leakage, sand content at 350 m and deformation at 260 m

Table 1 Geotechnical properties of the aeolian sand

Soil type	Natural density (g/cm^3)	Dry density (g/cm^3)	Void ratio	Hydraulic conductivity ($\times 10^{-3}$ cm/s)	Compression modulus (MPa)	Cohesion (kPa)	Internal friction angle (°)
Fine sand	1.59–1.70	1.53–1.64	0.56–0.82	1.1–2.5	19.42–25.32	0–8.35	32.20–36.45

gelation time measured at 7 °C, 12.5 °C, 18.2 °C, 22 °C, and 26 °C. The ambient temperature for the scale model test was 26 °C. When the mixing ratio of the modified urea–formaldehyde resin with 5% oxalic acid solution was 5:1, the gel time was 85 s.

Scale Model

The model was built to simulate the auxiliary inclined shaft of the Jinjitan coal mine, at the location illustrated in Figs. 1 and 2. The prototype has a length of ≈ 20 m along the inclined shaft and a width of 20 m from the center of the shaft tunnel. The height of the prototype reaches the ground surface, and a part of it was simulated by applying the cover pressure. The structure of the strata and grouting borehole layout in the prototype is also shown in the two figures. The geometric similarity ratio between the experimental model and the prototype is 1:20. The mechanical properties of the granular materials are mainly determined by the internal angle of friction of the material because its cohesion can be neglected. The similarity of the friction angle of the aeolian sand used in the experiment with that of sand aquifer ensured the reliability of the scale model test. The chemical grouts used in the experiment were the same as the grouts used in the Jinjitan coal mine. The confined aquifer between the two layers of clay was saturated before the test, and a water pressure of 11.0 kPa (1.1 m water head) was applied to simulate a pressure of 220 kPa (22 m of water head) in the prototype. The process of grouting into the saturated aeolian sand layer behind the auxiliary inclined shaft was simulated by drilling boreholes on the side wall of the shaft and grouting to control the water and sand inrush. The responses of the water pressures at different locations around the grouting boreholes behind the shaft wall and the pressures on the inner lining of side wall, floor, and roof were measured. Figure 4 shows the scale model design and a photograph of the set up. The size of the model chamber was 1.0 × 1.0 × 1.0 m in length × width × height, respectively. One side of the chamber was constructed with a circular arch and vertical wall to simulate half of the inclined shaft, due to its symmetry. The angle of the inclined shaft was adjusted to 5° using a jack. The floor of the chamber was made of a steel plate, and the four sides and shaft wall were made of transparent material to allow grout propagation to be observed. Figure 5 shows the model; the strata in the model was arranged in four layers, with an inclination of 0°. The soil layer to be grouted was a layer of fine sand taken from the site. The weathered sandstone rock mass was replaced by gravel. The loess consists of fine sand, and 5% lime powder was added to match the shear strength of the natural loess. Since the model was finite in height, a compensation load of 75 kPa (1.5 MPa in the prototype) was applied to the top of the model to achieve a similar vertical stress. Before the model was constructed, the required sand volume and density of each sand layer were calculated, and the layers were compacted to the specified height. After the layering was completed, the model was fully saturated. Table 2 lists the parameters of the strata in the model.

The grouting borehole was drilled at the center of the rib on the vertical side of the wall, and water pressure sensors were disposed 60 mm above and below the grouting borehole, and 50, 100, and 150 mm to the left and right of it. The membrane pressure sensors were embedded in the inner side of the shaft wall, at positions corresponding to the pore pressure observation points around the grouting borehole. Variations in the water pressure and pressure on the side wall, roof, and floor of the shaft were monitored during the grouting process. Figure 6 shows the layout and the numbering of sensors. The water pressure sensor was a voltage type operating within 0–0.1 MPa, and the frequency of the data logging instrument was set to 1 Hz. Pressures were obtained using a resistive membrane pressure sensor, and its acquisition frequency was also set to 1 Hz.

Two-Liquid Grouting Method

The two-liquid grouting pump operates with a pumping pressure between 0 and 4 MPa. By adjusting the number of injections of the two pumps, the grouting ratio between Liquids A and B can be adjusted. Before commencing the test, the data acquisition instrument was turned on, and 100 s of stable data were collected before the slurry was injected into the soil layer in chamber. The pumping pressure was measured until the grouting was completed (after ≈ 500 s). After the slurry was sufficiently solidified, the stabilized masses were peeled off to investigate the grout propagation.

Results and Analysis

Grouting Pressure

Figure 7 shows the pumping pressure during the experiment, which indicates that the grouting process was completed in three stages. In the first stage (100–170 s), the slurry began to enter the model, diffusing in at the contact surface between the outer wall of the model and the soil behind the wall. Since the resistance to be overcome by the diffusion of the slurry at this stage is small, the grouting pressure did not substantially change and was maintained at ≈ 196 kPa. In the second stage (170–420 s), the grouting pressure changed considerably, and pulsated since a manual grouting pump was used. At this stage, the gap behind the wall was completely filled by grout, and the slurry began to propagate into the soil layer behind the wall. In the third stage (420–500 s), the grouting pressure suddenly decreased and remained at

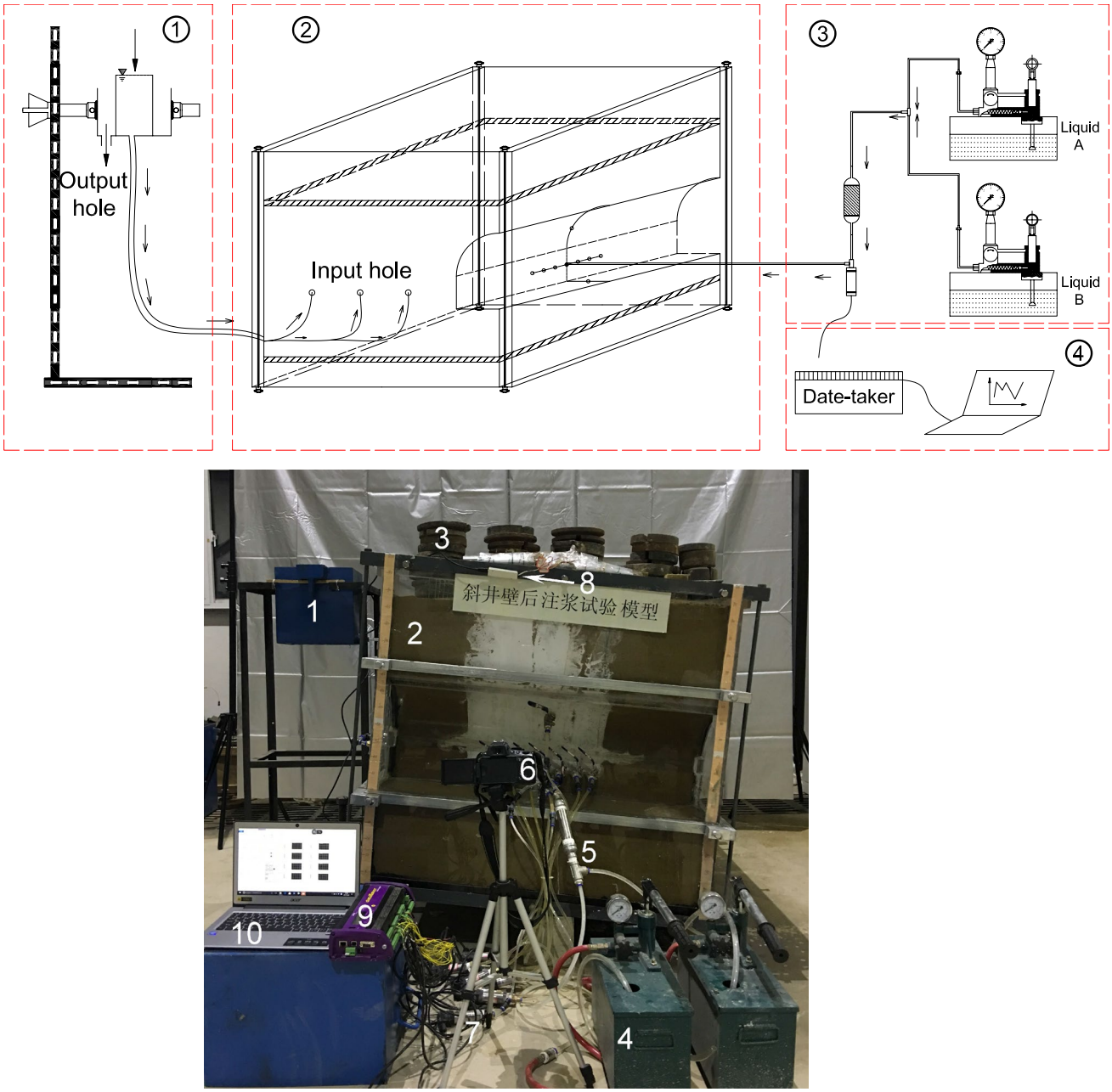

Fig. 4 Set up of the scale model for grouting behind shaft wall

a low value, mainly because the range of the diffusion of the slurry in the soil layer behind the wall had gradually expanded. This expansion allowed the slurry to come into contact with the model surface, and the grouting pressure to be dissipated toward the sides of the model.

Pressure on the Side Wall, Roof and Floor

Grout was injected for 100–500 s, after the measured pressures were stable for 100 s. After grouting, the pressures were continuously collected for 100 s. Then, the model was allowed to stand for 24 h. After the slurry fully solidified, the pressure was continuously monitored for 100 s. Figure 8 and Supplemental Fig. 6 show how the pressures on the side shaft wall increased after grouting began, and then decreased. These changes in the pressure on the shaft wall were closely related to the propagation of grout in the soil layer behind the wall. When the grouts penetrated and diffused in the soil layer, they drove free water from the pores, and the pressure began to increase. When the seepage pressure was at equilibrium with the pore water pressure, the grouts reached their maximum penetration length. At this

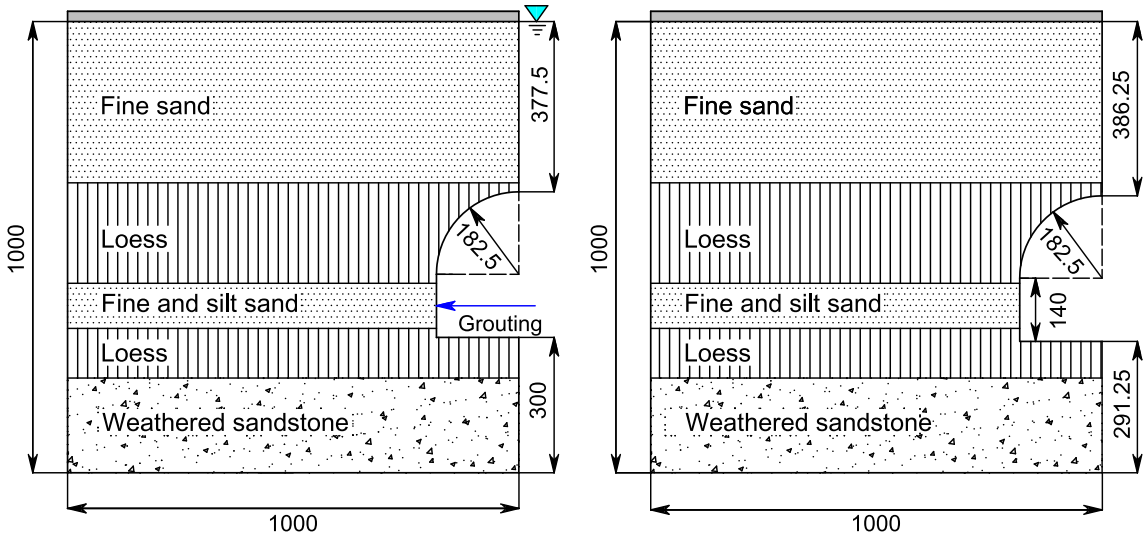

Fig. 5 Schematic of the model corresponding to cross section in Fig. 2

Table 2 Geotechnical parameters of soil in scale model

Layer	Thickness (cm)	Density (g/cm^3)	Cohesion (kPa)	Internal friction angle (°)
Fine sand	58	1.68	0	30
Loess	22.6	2.02	21.6	19.4
Fine and silt sand	10	1.88	2.05	23.0
Loess	11	2.02	21.6	19.4

point, the grouting pressure began to increase in the soil layer. When the grouting pressure was sufficient to overcome the principal stress of the soil layer, fractures were generated, which released pressure; consequently, the pressure on the wall dropped. As the slurry diffused into the periphery of the fractured grouting vein, the pressure accumulated again. After the slurry had fully solidified for 24 h, the pressure on the side wall still continued a slow release of ΔP, to less than before grouting.

Figure 9 and Supplemental Fig. 7 show the pressure variations in the roof of the inclined shaft at sensor no. 7. Three distinct peaks exist, with increasing peak pressure. At the initial stage of grouting at 100–200 s, the propagation of the slurry did not reach the roof, and the pressure on the roof remained almost unchanged. When the grouting was 200–330 s, the propagation range of the slurry in the soil layer behind the wall began to increase and change the pressure on the roof. When the grouting was at 330–500 s, the slurry spread to the roof driven by the grouting pressure. As slurry was continuously injected, the pressure increased. When the dominant diffusion path reached the top surface of the model, the pressure found a drainage pathway and suddenly dropped. When the slurry was fully solidified (24 h), the roof was also subjected to a sustained release of ΔP compared with before grouting, indicating that grouting also reduced the roof pressure of the inclined shaft.

The pressure on the floor of the inclined shaft during grouting was monitored by pressure sensors placed on the bottom of the test model. Figure 10 shows an increasing and decreasing trend of pressures on the floor. After 24 h, ΔP had increased compared with before grouting, which indicates that grouting into the side wall increased the pressure on the floor and caused swelling deformation of the inclined shaft floor.

Pore Water Pressure Behind the Shaft Wall

Figure 11 represents the pore water pressure measured behind the side wall after grouting. The grouting pressure first fluctuated with a low amplitude, then with a high amplitude, and then suddenly dropped. In the stage with low amplitude fluctuations, the slurry underwent permeation propagation, while in the stage with high amplitude fluctuations, the slurry underwent fracture and permeation propagation. As the slurry diffused into the pores of the sand layer behind the wall, it gradually replaced the free water in the pores. The slurry gradually solidified, and the pore water pressure gradually decreased. When the slurry spread to the top surface of the model, the pressure was released via the drainage pathway.

Figure 12 shows that the pore water pressure behind the roof exhibited three very similar stages. However, its low-amplitude fluctuation phase lasted longer than the high-amplitude fluctuation phase because the slurry required time to diffuse from the side to the roof, while

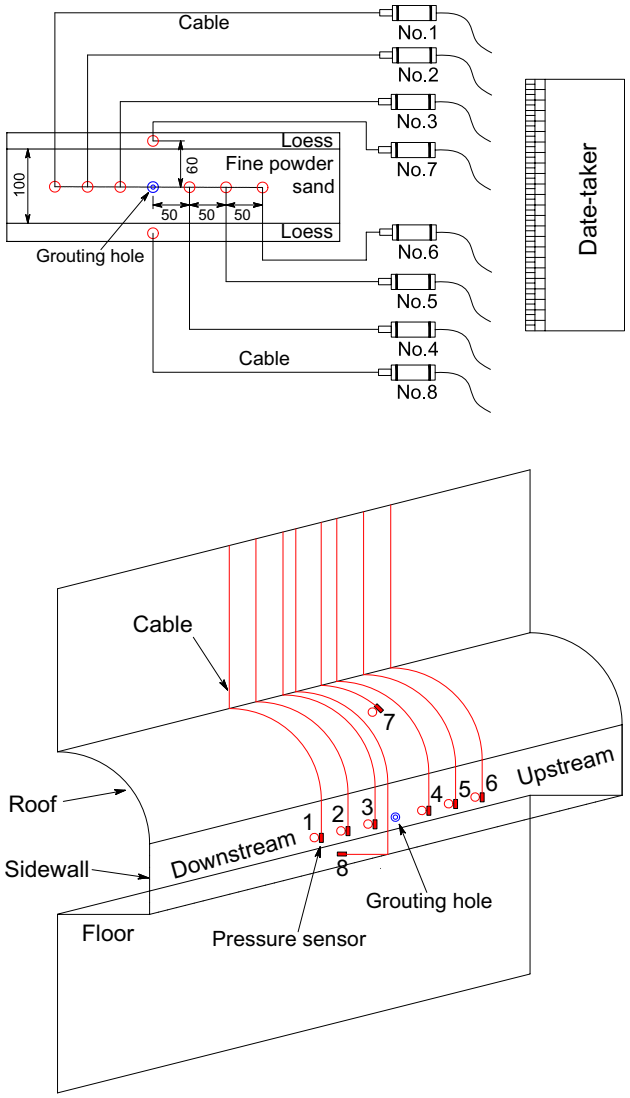

Fig. 6 Layout of water pressure sensors and pressure sensors

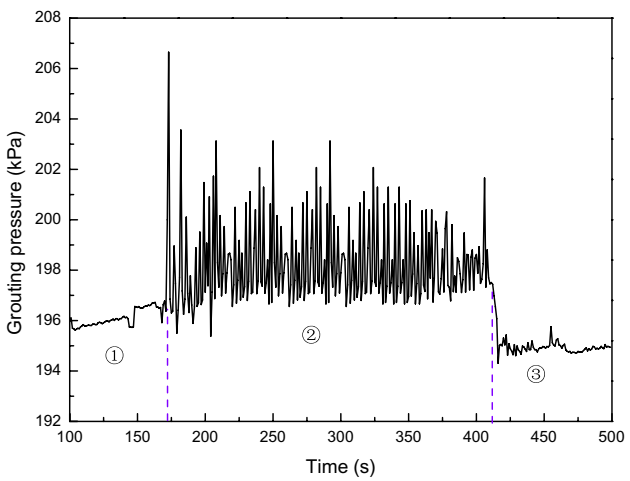

Fig. 7 Grouting pressure

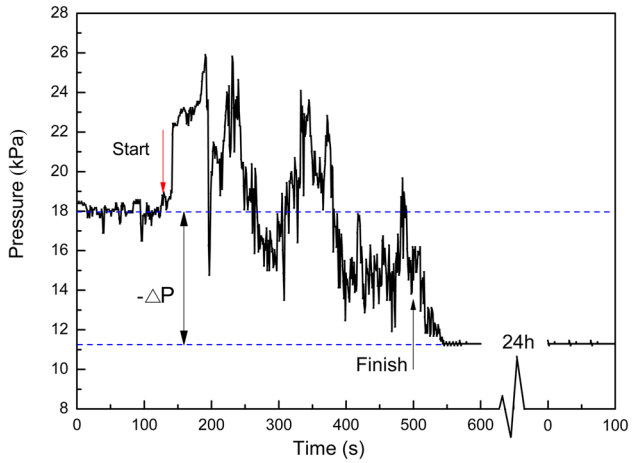

Fig. 8 Pressure–time curves of pressure sensors no. 1 on the side wall

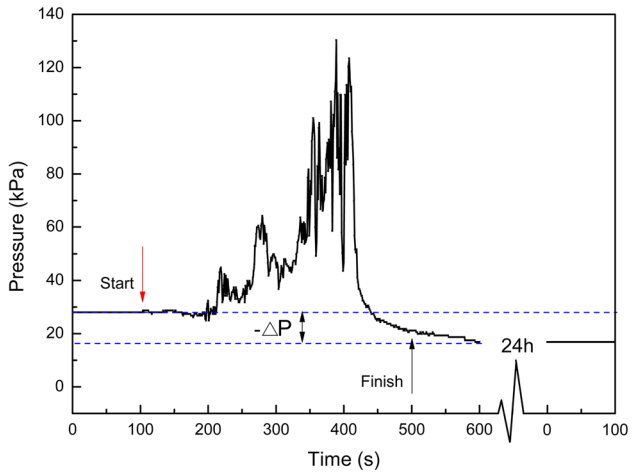

Fig. 9 Pressure–time curve of pressure sensor no. 7 on the roof

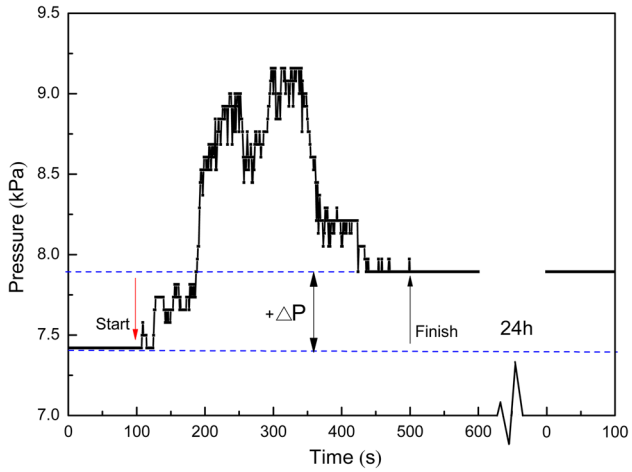

Fig. 10 Pressure-time curve of pressure sensor no. 8 on the floor

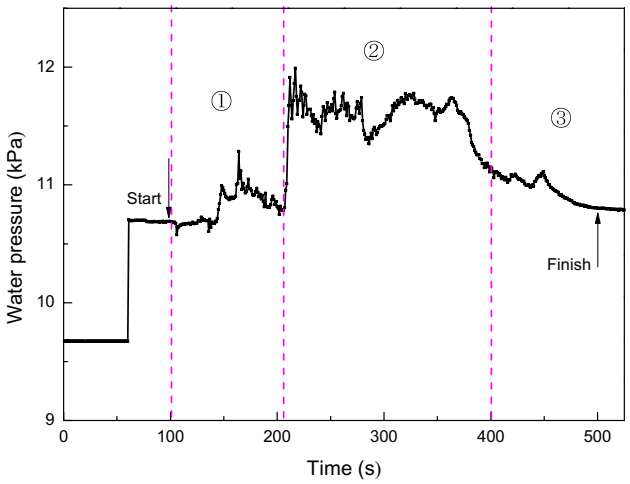

Fig. 11 Pore water pressure–time curve of water pressure sensor no. 1 on the side wall

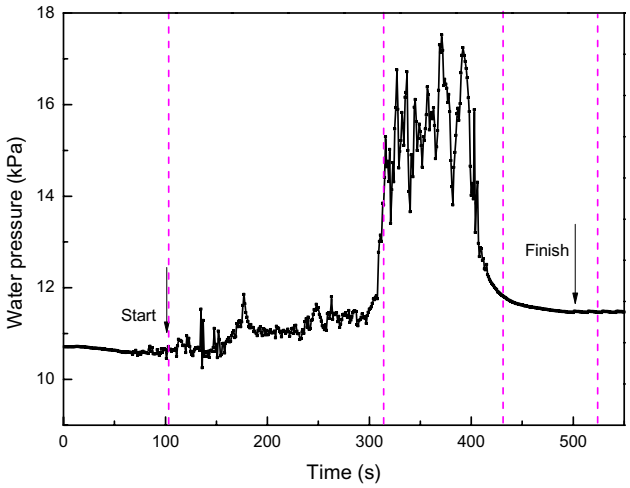

Fig. 12 Pore water pressure–time curve of water pressure sensor no. 7 on the roof

the distance between the roof and top surface of the model was short. When the slurry and the top surface of the model formed a pressure relief pathway, the pore water pressure suddenly dropped.

Figure 13 shows that the pore water pressure against the floor exhibited three different stages, namely, pressure surge, maintenance, and recovery, which is opposite to the pore water pressure responses of the side and roof. The pore water pressure of the floor suddenly increased after grouting commenced. Then, the pressure sharply decreased and remained constant at a low value. The pressure increased slightly at the end of the grouting.

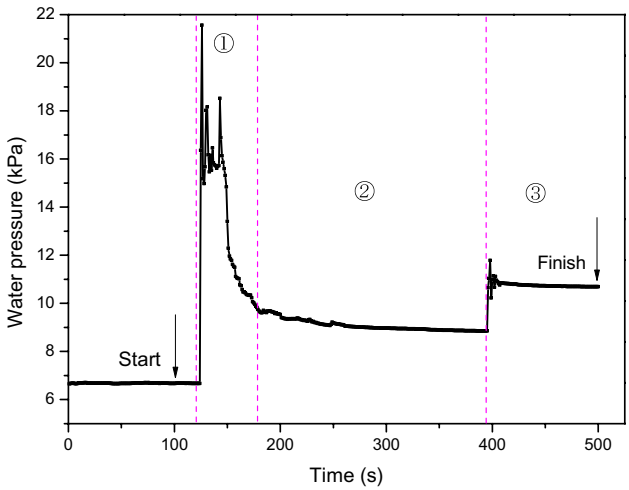

Fig. 13 Pore water pressure–time curve of water pressure sensor no. 8 on the floor

Discussion

Pressure and Pore Water Pressure Changes During Grouting

The experimental results show that during the grouting process, the side wall and roof of the inclined shaft experienced several changes of increasing and decreasing pressure. Each such change in pressure was closely related to the way the grout propagated behind the inclined shaft wall. At the end of grouting, after the grouts fully gelled, the pressure on the side wall and roof was reduced, while that on the floor was increased. The vertical pressure on the side wall and roof was taken up by the equivalent shaft wall, which was formed by the grouted stabilized mass, and reduced the stress on the side wall and roof. After the sand layer behind the inclined shaft was filled with grout, the pressure on the floor increased. Thus, curtain grouting reinforced the ruptured wall, sealed the water and sand pathways, and bore the increased vertical stress.

The water pressure in the aquifers near the side wall of the inclined shaft and the roof experienced three stages: low amplitude fluctuations, high amplitude fluctuations, and a sudden drop. In contrast, the water pressure in the aquifers near the floor experienced stages of pressure surge, maintenance, and recovery. The process of grouting behind the inclined shaft wall constantly disturbed the strata and aquifer and increased the burden on the shaft wall. Therefore, the grouting parameters should be strictly controlled to prevent secondary damage.

This study showed that the pressure increase on the floor was greater than that on the side wall and roof. This implies that the grouting pressure in the floor should be slightly less than that in the roof and side wall, in order to avoid

secondary failure of the floor. In the treatment of the accident, initially, the designed grouting pressure was selected to be same at less than 1 MPa for the roof, side wall, and floor. However, it was found that the heaving and fracture of the floor was more serious than in the side wall and roof. When the grouting pressure was greater than 0.5 MPa, the speed of heaving and fracture accelerated. In the second stage of treatment, the final grouting pressure for the roof and side wall was strictly controlled below 0.8 MPa (less than 1.2 MPa instantly) and that for the floor was strictly controlled below 0.5 MPa (less than 0.8 MPa instantly). There was no obvious rupture or cracking during the grouting process. Certainly, the pressure and water pressure on the shaft wall and in the aquifers should be closely monitored to prevent secondary damage by grouting.

Stabilization Effect of Grouting for an Inclined Shaft Wall

The vertical additional pressure acts directly on the outer shaft wall before grouting. After grouting, the vertical additional pressure is partially exerted on the grout curtain, which is equivalent to increasing the thickness of the wall from d to d' (Supplemental Fig. 8). The vertical additional pressure is transferred from the original wall to the equivalent wall, thereby protecting the ruptured wall. Without grouting, the free surface of the floor of the inclined shaft is subjected to upward pressure. When the pores of the sand layer on the inclined shaft are filled with grout, the pressure on the floor increases. After the slurry is fully solidified to a certain thickness on the shaft wall, the ruptured wall is reinforced and the water and sand flow ceases. To form an effective grouting curtain, parameters such as the grouting pressure, grout take, and slurry ratio, should be strictly controlled during grouting. The water inflow rate, wall displacement, water pressure, noise, and other parameters should be monitored during the grouting process to ensure well-dispersed grouts and shaft wall safety.

Propagation Zoning

Supplemental Figure 9a shows the solidified grouted sand removed from the mold after 48 h of grouting. The solidified grouted sand had an irregular shape, with smooth protrusions on its surface. The maximum vertical height was ≈ 35.25 cm, the horizontal maximum length was 42.0 cm, and the maximum width was 38.5 cm. To more closely observe grout propagation, the grouted sand mass was sliced horizontally from the top, and images were captured every 1.5 cm. Supplemental Figure 9b shows the relative position between each slice image and the shaft wall. A total of 20 slice images were collected; Supplemental Figure 9c shows some typical slice images.

Figure 14 shows a speculated propagation pattern of the chemical grouts, which is mainly dominated by fracturing and permeating grouting. Two mutually perpendicular splitting planes are indicated, parallel and perpendicular to the shaft wall. The initial fracture surface occurs on the acting plane of the minimum principal stress and gradually solidifies as the slurry penetrates both sides of the fracture. A sol-based chemical slurry, rather than granular slurry, is more likely to infiltrate and diffuse into the pores. On both sides of the fracture, the sand particles are clearly cemented. Therefore, the diffusion and sand-fixing method of the chemical slurry is a coupling of fracturing and permeation. The penetration length of the chemical slurry is divided into three segments with different sand-fixing modes according to the contact pattern of particles, as shown in Fig. 14: (1) slurry as a skeleton: this area is mainly distributed in the interior of the cleavage vein. The sand particles are suspended in the slurry and separated from each other, and the strength and impermeability are mainly based on the slurry skeleton. (2) Granular particle and slurry as a skeleton: this area is mainly distributed in the area close to both sides of the fracture. An obviously high slurry concentration can be observed in this zone, and the slurry is filled between the particles, both in the particle and slurry skeletons. (3) Granular particle as a skeleton: this area is mainly distributed on the outer edge of the grouted solidified mass. This part contains less slurry with only a small section of filled pores. The consolidation strength is low. The sand particles are in contact with each other, and the sand skeleton is almost unchanged by grouting.

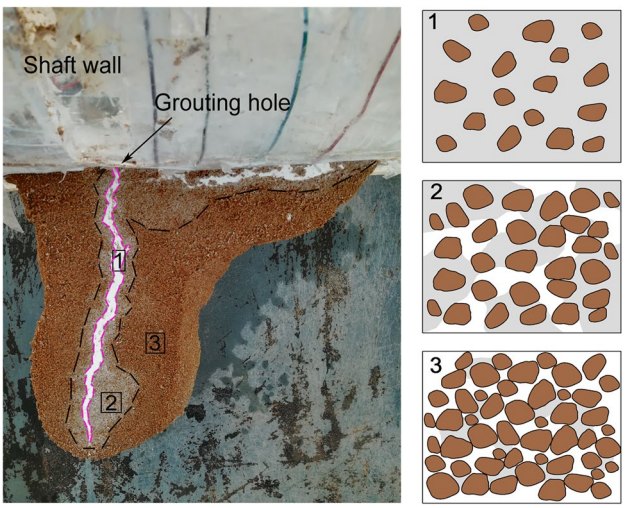

Fig. 14 Three patterns of propagation

Limitations

The main focus of this study was the mechanical aspects of grouting pressure design. Chemical issues were not investigated but will be a topic of future studies. To simplify the experiment, the combination of inrush and grouting were not simulated; the simulation of water and sand mixture inrushing would be much more difficult. The subject of grouting into aquifers with flowing water can be found in the literature. Furthermore, multi-hole grouting at different positions was not simulated, and remains for further study.

Conclusion

The experimental results from the scale model test of grouting in aquifers surrounded an inclined shaft revealed pressure and water pressure changes during grouting, with some implications for grouting pressure design. The main conclusions are as follows:

1. The pressure on the side wall and roof of the inclined shaft exhibited several changes in magnitude during grouting. The pressure increased when the grout propagation was permeating, and decreased when it was fracturing. At the end of grouting, the pressure on the sides and roof decreased and that on the floor increased. Grouting practice also shows that heaving and cracking in the floor are more obvious than in the side wall and roof. This implies that the grouting pressure in the floor should be less than that in the roof and side wall to avoid secondary failure of the floor. In fact, grouting in the Jinjitan coal mine confirmed this conclusion.
2. The pore water pressure in the aquifer behind the side wall and roof of the inclined shaft exhibited three different stages: low amplitude fluctuations, high amplitude fluctuations, and a sudden drop. In contrast, the water pressure on the floor experienced a pressure surge, maintenance, and recovery. The process of grouting behind the inclined shaft wall is a constant disturbance to the strata and aquifer and changes the pore water pressure. The result also shows that the water pressure increase in the aquifers surrounding the floor is greater than in the side wall and roof, which further demonstrates that the grouting pressure in the floor should be less than in the roof and side wall to avoid secondary failure.
3. The results of this study also show that the pressure acting on the shaft wall and the pore water pressure in the aquifers surrounding the shaft obviously change during grouting. From the perspective of grout propagation and the sealing effect, increased grouting pressure is beneficial to longer propagation, but the adverse effect of high-pressure grouting on the shaft wall also increases. Therefore, grouting pressures should fully consider the amount of pressure on the shaft wall. Grouting parameters, such as pressure and pore water pressure, should be strictly controlled, and the response of the shaft wall should be monitored to prevent secondary damage.

Acknowledgements The authors thank the National Natural Science Foundation of China (Grant 41877238) for its financial support.

References

Amadei B, Savage WZ (2001) An analytical solution for transient flow of Bingham viscoplastic materials in rock fractures. Int J Rock Mech Min Sci 38(2):285–296

Castro RL, Basaure K, Palma S, Vallejos J (2017) Geotechnical characterization of ore related to mud rushes in block caving mining. J S Afr Inst Min Metall 117(3):275–284

Cheng W, Ni J, Shen J, Wang Z (2018) Modeling of permeation and fracturing grouting in sand: laboratory investigations. J Test Eval 46(5):2067–2082

Cochard S, Ancey C (2009) Experimental investigation of the spreading of viscoplastic fluids on inclined planes. J Non-Newton Fluid Mech 158(1–3):73–84

Cui GX (1998) Failure mechanism and prevention techniques of vertical shaft wall in special formation conditions. Mine Constr Technol 19(1):28–32 **(in Chinese)**

Dai G, Bird RB (1981) Radial flow of a Bingham fluid between two fixed circular disks. J Non-Newton Fluid 8(3):349–355

Funehag J, Thörn J (2018) Radial penetration of cementitious grout—laboratory verification of grout spread in a fracture model. Tunn Undergr Space Technol 72:228–232

Gustafson G, Claesson J, Fransson Å (2013) Steering parameters for rock grouting. J Appl Math 2013:1–9

Guo MW (2010) Experimental study on diffusion mechanism of chemical slurry in porous media with high pressure closed environment. China Univ of Mining and Technology, Xuzhou, pp 39–132 **(in Chinese, abstract in English)**

Haza ZF, Harahap ISH, Dakssa LM (2013) Experimental studies of the flow-front and drag forces exerted by subaqueous mudflow on inclined base. Nat Hazards 68(2):587–611

Håkansson U (1993) Rheology of fresh cement-based grouts. Royal Institute of Technology, Stockholm

Karol RH (2003) Chemical grouting and soil stabilization, 3rd edn. Marcel Dekker-Taylor and Francis, New York

Krizek RJ, Perez T (1985) Chemical grouting in soils permeated by water. J Geotech Eng 111(7):898–915

Liang YK, Sui WH, Qi JF (2019) Experimental investigation on chemical grouting of inclined fracture to control sand and water flow. Tunn Undergr Space Technol 83:82–90

Luo PP, Li SY, Fan B (2009) Study on flow model for Binghamian grouts in tilted single fracture. Mem Muroran Inst Tech 59:207–211

Maag E (1938) Ueber die Verfestigung und Dichtung des Baugrundes (Injektionen). Erdbaukurs de ETH, Sammlung der Vorträge herausgegeben vom Institut für Erdbauforschung der eidg. Techn Hochschule Zürich, Zürich

Minto JM, MacLachlan E, Mountassir GE, Lunn RJ (2016) Rock fracture grouting with microbially induced carbonate precipitation. Water Resour Res 52(11):8827–8844

Mohammed M, Pusch R, Knutsson S (2015) Study of cement-grout penetration into fractures under static and oscillatory conditions. Tunn Undergr Space Technol 45:10–19

Ni XH, Sui WH, Guan YZ, Wang DL, Du Y (2005) Research on prevention and control technology of shaft rupture in coal mine shaft. China Univ of Mining and Technology Press, Xuzhou **(in Chinese)**

Qian ZW, Jiang ZQ, Guan YZ, Yue N (2018) Mechanism and remediation of water and sand inrush induced in an inclined shaft by large-tonnage vehicles. Mine Water Environ 37(4):849–855

Ruan WJ (2005) Research on diffusion of grouting and basic properties of grouts. Chin J Geotech Eng 27(1):69–73 **(in Chinese, abstract in English)**

Sui WH, Liu JY, Hu W, Qi JF, Zhan KY (2015) Experimental investigation on sealing efficiency of chemical grouting in rock fracture with flowing water. Tunn Undergr Space Technol 50:239–249

Vallejos J, Basaure K, Palma S, Castro RL (2017) Methodology for evaluation of mud rush risk in block caving mining. J S Afr Inst Min Metall 117(5):491–497

Wang DL (2011) Mechanism of hydro-dynamically chemical grouting in porous media. China Univ of Mining and Technology, Xuzhou **(in Chinese, abstract in English)**

Xiao F, Zhao Z, Chen H (2017) A simplified model for predicting grout flow in fracture channels. Tunn Undergr Space Technol 70:11–18

Xu Y, Du M, Luo Y (2019) Using water injection to prevent shaft failure in the Jining no. 3 coalmine, China. Mine Water Environ 38(1):60–71

Xu Z, Liu C, Zhou X, Gao G, Feng X (2019) Full-scale physical modelling of fissure grouting in deep underground rocks. Tunn Undergr Space Technol 89:249–261

Yu W, Li P, Zhang X, Wang Q (2014) Model test research on hydrodynamic grouting for single fracture with variable inclinations. Rock Soil Mech 35(8):2137–2143 **(in Chinese, abstract in English)**

Yuan SC, Zhang GL, Zheng GS, Cai FH, Qian ZW (2018) Grouting treatment of water and sand inrush into an inclined shaft in aeolian sand layer. J China Coal Soc 43(4):1104–1110 **(in Chinese, abstract in English)**

Yuan SC, Zheng GS, Qian ZW, Cai FH (2019) Research on water and sand inrush mechanism and repair technology of shaft rupture in inclined shaft. Coal Sci Technol 47(5):113–118 **(in Chinese, abstract in English)**

Zhang GL (2011) High-pressure permeability and microscopic mechanism of chemical grouting solid sand body. China Univ of Mining and Technology, Xuzhou, pp 46–80 **(in Chinese, abstract in English)**